Inorg. Chem. **XXXX**, *xx*, 0

Synthesis and Reactivity of the Aquation Product of the Antitumor Complex *trans*-[$Ru^{III}Cl_4$(indazole)$_2$]$^-$

Berta Cebrián-Losantos,[†] Erwin Reisner,[†,‡] Christian R. Kowol,[†] Alexander Roller,[†] Sergiu Shova,[§] Vladimir B. Arion,*[,†] and Bernhard K. Keppler*[,†]

Institute of Inorganic Chemistry, University of Vienna, Währingerstr. 42, A-1090 Vienna, Austria, Inorganic Chemistry Laboratory, University of Oxford, South Parks Road, OX1 3QR Oxford, U.K., and Department of Chemistry, Moldova State University, A. Mateevici Street 60, 2009 Chisinau, Moldova

Received March 20, 2008

Aquation of the investigational anticancer drug *trans*-[$Ru^{III}Cl_4$(Hind)$_2$]$^-$ (**1**, KP1019) results in the formation of *mer,trans*-[$Ru^{III}Cl_3$(Hind)$_2$(H_2O)] (**2**), which was isolated in high yield (85%) and characterized by spectroscopic methods and X-ray crystallography. Dissolution of **2** in acetone, led to its dimerization into [Ru^{III}_2(μ-Cl)$_2$$Cl_4$(Hind)$_4$]·2(Me)$_2$CO (**3**) in 79% yield, with release of two water molecules. Complex **2** reacts readily with nucleophilic organic molecules, viz., methanol or dimethyl sulfide, at room temperature by replacement of the aqua ligand to give *mer,trans*-[$Ru^{III}Cl_3$(Hind)$_2$(MeOH)] (**4**) and *mer,trans*-[$Ru^{III}Cl_3$(Hind)$_2$(Me_2S)] (**5**) in 58 and 64% yield, respectively. By reaction of **2** with DMSO at room temperature or dimethyl sulfide at elevated temperatures *trans,trans,trans*-[$Ru^{II}Cl_2$(Hind)$_2$(Me_2S)$_2$] (**6**) and *trans,trans,trans*-[$Ru^{II}Cl_2$(Hind)$_2$(*S*-DMSO)$_2$] (**7**) were prepared in 64 and 75% yield, respectively. Dissolution of **2** in acetonitrile or benzonitrile gave rise to *mer,trans*-[$Ru^{III}Cl_3$(Hind)(HN=C(Me)ind)] (**8a**), *mer,trans*-[$Ru^{III}Cl_3$(Hind)(HN=C(Ph)ind)] (**8b**), and *trans,trans*-[$Ru^{III}Cl_2$(HN=C(Me)ind)$_2$]Cl (**9**) in 67, 50, and 23% yield, respectively, upon metal-assisted iminoacylation of indazole, which is unprecedented for ruthenium(III). Furthermore, complex **2** reacts with the DNA-model bases 9-methyladenine (9-meade) and *N6,N6*-dimethyladenine (6-me_2ade) to yield *mer,trans*-[$Ru^{III}Cl_3$(Hind)$_2$(9-meade)] (**10**) and *mer,trans*-[$Ru^{III}Cl_3$(Hind)$_2$(6-me_2ade)] (**11**) with the purine bases bound to the Ru(III) center via N7 and N3, respectively. Complex **11** represents the first ruthenium complex in which the coordination of the purine ligand *N6,N6*-dimethyladenine occurs via N3. In addition, the polymer [Na(EtOAc)$_2$$Ru^{III}$($\mu$-Cl)$_4$(Hind)$_2$]$_n$ (**12**) was crystallized from ethyl acetate/diethyl ether solutions of Na[*trans*-$Ru^{III}Cl_4$(Hind)$_2$]·1.5H_2O (**1a**). The reported complexes were characterized by elemental analysis, IR and UV−vis spectroscopy, ESI mass spectrometry, cyclic voltammetry, and X-ray crystallography. Electrochemical investigations give insight into the mechanistic details of the solvolytic behavior of complex **2**. The lability of the aqua ligand in **2** suggests that this complex is a potential active species responsible for the high antitumor activity of *trans*-[$Ru^{III}Cl_4$(Hind)$_2$]$^-$.

Introduction

The development of metallopharmaceuticals is a frontier area in bioinorganic chemistry,[1] and ruthenium(II)- and ruthenium(III)-based compounds with a classical coordination sphere, as well as organometallic complexes, are the subject of current investigation as promising anticancer drug candidates (Figure 1).[2,3] Two of these ruthenium complexes, viz., *trans*-[$Ru^{III}Cl_4$(L)(L′)]$^-$ (L = L′ = indazole = Hind) for KP1019[4] (Figure 1a), and (L = imidazole, L′ =

* To whom correspondence should be addressed. E-mail: vladimir.arion@univie.ac.at (V.B.A.), bernhard.keppler@univie.ac.at (B.K.K.). Phone: +431427752600. Fax: +431427752680.
† University of Vienna.
‡ University of Oxford.
§ Moldova State University.

(1) (a) Special issue of Chemical Reviews dedicated to Medicinal Inorganic Chemistry: *Chem. Rev.* **1999**, *99*, 2201−2842. Introduction by the editors: C. Orvig, M. J. Abrams, *Chem. Rev.* **1999**, *99*, 2201. (b) Guo, Z.; Sadler, P. J. *Angew. Chem., Int. Ed.* **1999**, *38*, 1512–1531.
(2) Clarke, M. J. *Coord. Chem. Rev.* **2003**, *236*, 209–233.
(3) (a) Ang, W. H.; Dyson, P. J. *Eur. J. Inorg. Chem.* **2006**, 4003–4018. (b) Ang, W. H.; Daldini, E.; Scopelliti, R.; Juillerat-Jeannerat, L.; Dyson, P. J. *Inorg. Chem.* **2006**, *45*, 9006–9013. (c) Gossens, C.; Dorcier, A.; Dyson, P. J.; Rothlisberger, U. *Organometallics* **2007**, *26*, 3965–3975. (d) Dyson, P. J.; Sava, G. *Dalton Trans.* **2006**, 1929–1933.
(4) Hartinger, C. G.; Zorbas-Seifried, S.; Jakupec, M. A.; Kynast, B.; Zorbas, H.; Keppler, B. K. *J. Inorg. Biochem.* **2006**, *100*, 891–904.

10.1021/ic800506g CCC: $40.75
Published on Web 06/14/2008

S-DMSO) for NAMI-A[5] (Figure 1b), recently finished successfully phase I clinical trials. The prodrug *trans*-$[Ru^{III}Cl_4(Hind)_2]^-$ is active as an anticancer agent against primary tumors and metastases and, in particular, colon carcinomas.[6] Although its antitumor activity has been reported in the 1980s, the mechanism of action is largely not understood at the molecular level, and the identification of its active species is of major interest. So far much emphasis has been placed on: (i) aquation reactions in biologically relevant media and identification of products formed,[7] (ii) the establishment of structure/electrochemical property relationships regarding the "activation by reduction" hypothesis,[8] (iii) protein binding studies with serum proteins,[9] and (iv) interaction with relevant biological targets (e.g., nucleotides).[10] These aspects are closely linked together and may contribute to the understanding of the mechanism of action of ruthenium(III) prodrugs and elucidating the active species of *trans*-$[Ru^{III}Cl_4(L)(L')]^-$ complexes.

Aqua-species formed after administration of metalloprodrugs in vivo, for example, for *cis*-$[PtCl_2(NH_3)_2]$ (cisplatin),[11] play a critical role as (re)active species, being generally orders of magnitude more labile than the corresponding chlorido compounds.[12] Metal complexes that aquate readily are often cytotoxic, whereas inert complexes are only weakly active or inactive.[13] The importance of aquation for ruthenium species has been recently demonstrated for a series of $[Ru^{II}(\eta^6\text{-arene})(ethylenediamine)(X)]^{n+}$ compounds (Figure 1c), where the rate of substitution of the leaving group X by water molecules generally correlates with their antineoplastic activity against A2780 human ovarian cancer cells.[13] (H_2ind)-[*trans*-$Ru^{III}Cl_4(Hind)_2$] is stable in the solid state and the original complex aquates slowly with a pseudo-first rate constant of $k = 0.395 \pm 0.014 \cdot 10^{-5}$ s^{-1} at 25 °C in water.[7] However, increasing labilization takes place in physiological buffer solutions (37 °C, pH 7.4), and replacement of chlorido ligands by water has been suggested for *trans*-$[Ru^{III}Cl_4(Hind)_2]^-$. Despite the plethora of investigations of aquation reactions of KP1019 and NAMI-A, no products have been isolated and characterized in the solid state so far precluding studies of the potentially active monoaqua species.

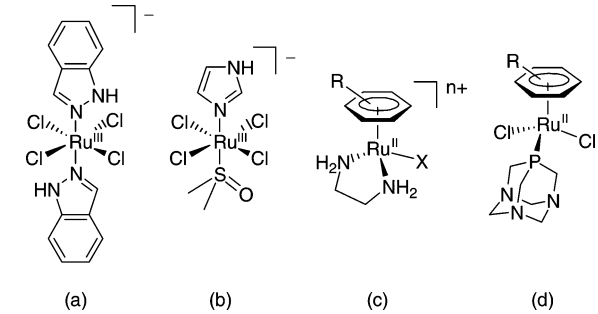

Figure 1. Chemical structures of promising ruthenium drug candidates under current investigation: (a) the anion of (H_2ind)[*trans*-$Ru^{III}Cl_4(Hind)_2$] (KP1019), (b) the anion of (H_2im)[*trans*-$Ru^{III}Cl_4(Him)$(*S*-DMSO)] (NAMI-A), (c) the cation of the piano-stool complex $[Ru^{II}(\eta^6\text{-arene})(ethylenediamine)(X)]^{n+}$, and (d) RAPTA-type complexes.

Herein we report on the synthesis and full characterization of *mer,trans*-$[Ru^{III}Cl_3(Hind)_2(H_2O)]$ (**2**), which is formed by aquation reaction of *trans*-$[Ru^{III}Cl_4(Hind)_2]^-$ (**1**). The X-ray diffraction structure of **2** and the reactivity of this complex toward a number of nucleophilic molecules and DNA model bases 9-methyladenine (9-meade) and *N6,N6*-dimethyladenine (6-me$_2$ade) was investigated and compared with that of **1**. Solvolysis of **2** in different solvents results in (i) dimerization in weakly coordinating solvents, for example, tetrahydrofuran (THF) or acetone, with release of two water molecules (ii) replacement of the aqua ligand by good donor molecules, for example, MeOH or Me_2S, (iii) coordination of two S-ligands (DMSO and Me_2S) and reduction to ruthenium(II), and (iv) formation of amidine-chelates in MeCN or PhCN. In addition, complexes **1** and **2** react with 9-meade and 6-me$_2$ade to yield *mer,trans*-$[Ru^{III}Cl_3(Hind)_2(\kappa^{N7}$-9-meade)] (**10**) and *mer,trans*-$[Ru^{III}Cl_3(Hind)_2(\kappa^{N3}$-6-me$_2$ade)] (**11**). All products have been studied in detail by spectroscopic, electrochemical, and X-ray diffraction methods.

Experimental Section

Synthesis of Complexes. Dimethyl sulfide was purchased from Aldrich and used as received. (Me_4N)[*trans*-$Ru^{III}Cl_4(Hind)_2$],[14] Na[*trans*-$Ru^{III}Cl_4(Hind)_2]\cdot 1.5H_2O$ (**1a**, KP1339),[14] 9-methyladenine (9-meade),[15] and *N6,N6*-dimethyladenine (6-me2ade)[16] were prepared as described elsewhere. Complexes *trans,trans,trans*-$[Ru^{II}Cl_2(Hind)_2(Me_2S)_2]$ (**6**, Yield: 64%),[17] *trans,trans,trans*-

(5) (a) Rademaker-Lakhai, J. M.; Van Den Bongard, D.; Pluim, D.; Beijnen, J. H.; Schellens, J. H. M. *Clin. Cancer Res.* **2004**, *10*, 3717–3727. (b) Alessio, E.; Mestroni, G.; Bergamo, B.; Sava, G. *Curr. Top. Med. Chem.* **2004**, *4*, 1525–1535.
(6) Berger, M. R.; Garzon, F. T.; Keppler, B. K.; Schmähl, D. *Anticancer Res.* **1989**, *9*, 761–765.
(7) (a) Küng, A.; Pieper, T.; Wissiack, R.; Rosenberg, E.; Keppler, B. K. *J. Biol. Inorg. Chem.* **2001**, *6*, 292–299. (b) Pieper, T.; Peti, W.; Keppler, B. K. *Met.-Based Drugs* **2000**, *7*, 225–232.
(8) Reisner, E.; Arion, V. B.; Keppler, B. K.; Pombeiro, A. J. L. *Inorg. Chim. Acta* **2008**, *361*, 1569–1583.
(9) Timerbaev, A. R.; Hartinger, C. G.; Aleksenko, S. S.; Keppler, B. K. *Chem. Rev.* **2006**, *106*, 2224–2248.
(10) (a) Küng, A.; Pieper, T.; Keppler, B. K. *J. Chromatogr. B* **2001**, *759*, 81–89. (b) Schluga, P.; Hartinger, C. G.; Egger, A.; Reisner, E.; Galanski, M.; Jakupec, M. A.; Keppler, B. K. *Dalton Trans.* **2006**, 1796–1802.
(11) (a) *Cisplatin: Chemistry and Biochemistry of a Leading Anticancer Drug, Helvetica Chimica Acta, Zürich*; Lippert B. , Ed.; Wiley VCH: Weinheim, 1999. (b) Wang, E. D.; Lippard, S. J. *Nat. Rev. Drug Discovery* **2005**, *4*, 307–320. (c) Wong, E.; Giandomenico, C. M. *Chem. Rev.* **1999**, *99*, 2451–2466.
(12) (a) Suvachittanont, S.; Van Eldik, R. *Inorg. Chem.* **1994**, *33*, 895–904. (b) Hohmann, H.; Van Eldik, R. *Inorg. Chim. Acta* **1990**, *174*, 87–92.
(13) Wang, F.; Habtemariam, A.; van der Geer, E. P. L.; Fernandez, R.; Melchart, M.; Deeth, R. J.; Aird, R.; Guichard, S.; Fabbiani, F. P. A.; Lozano-Casal, P.; Oswald, I. D. H.; Jodrell, D. I.; Parsons, S.; Sadler, P. J. *Proc. Natl. Acad. Sci. U.S.A.* **2005**, *102*, 18269–18274.
(14) Peti, W.; Pieper, T.; Sommer, M.; Keppler, B. K.; Giester, G. *Eur. J. Inorg. Chem.* **1999**, 1551–1555.
(15) (a) Talman, E. G.; Bruening, W.; Reedijk, J.; Spek, A. L.; Veldman, N. *Inorg. Chem.* **1997**, *36*, 854–861. (b) Charland, J. P.; Phan Viet, M. T.; St-Jacques, M.; Beauchamp, A. L. *J. Am. Chem. Soc.* **1985**, *107*, 8202–8211.
(16) Itaya, T.; Matsumoto, H.; Ogawa, K. *Chem. Pharm. Bull.* **1980**, *28*, 1920–1924.
(17) (a) Egger, A.; Arion, V. B.; Reisner, E.; Cebrián-Losantos, B.; Shova, S.; Trettenhahn, G.; Keppler, B. K. *Inorg. Chem.* **2005**, *44*, 122–132. (b) Egger, A. Diploma Thesis, University of Vienna, Vienna, Austria, 2004; p 89.

[Ru^{II}Cl$_2$(Hind)$_2$(*S*-DMSO)$_2$] (**7**, Yield: 75%),[18] and *mer,trans*-[Ru^{III}Cl$_3$(Hind)$_2$(9-meade)] (**10**, Yield: 68% from MeOH at 60 °C)[17] were isolated similarly to literature procedures using *mer,trans*-[Ru^{III}Cl$_3$(Hind)$_2$(H$_2$O)] (**2**) as the starting material instead of *trans*-[Ru^{III}Cl$_4$(Hind)$_2$]$^-$ (**1**). The synthesis of *mer,trans*-[Ru^{III}Cl$_3$(Hind)$_2$(κ^{N3}-6-me$_2$ade)] (**11**) was performed by taking into account previous experience on the reactivity study of **1** toward *N6,N6*-dimethyladenine.[17b] The composition of the products was confirmed by elemental analysis, IR spectroscopy, and ESI mass spectrometry. Crystals of [Na(EtOAc)$_2$Ru^{III}Cl$_4$(Hind)$_2$]$_n$ (**12**) have been isolated upon recrystallization of Na[*trans*-Ru^{III}Cl$_4$(Hind)$_2$] (**1a**) in EtOAc/Et$_2$O at 4 °C.

***mer,trans*-[Ru^{III}Cl$_3$(Hind)$_2$(H$_2$O)] (2).** Indazole (0.10 g, 0.85 mmol) was dissolved in diluted aqueous HCl (400 mL, 2 mM) under heating to 80 °C. The resulting solution was cooled to room temperature, and a solution of Na[*trans*-Ru^{III}Cl$_4$(Hind)$_2$]·1.5H$_2$O (**1a**) (0.45 g, 0.85 mmol) in H$_2$O (100 mL) was added under stirring. The reaction mixture was allowed to stand at room temperature, and after two days, red crystals formed, were filtered off, washed with water, and dried in vacuo at room temperature. Yield: 0.34 g, 85%. Anal. Calcd for C$_{14}$H$_{14}$Cl$_3$N$_4$ORu (M_r = 461.71 g/mol): C, 36.42; H, 3.06; N, 12.13; Cl, 23.03. Found: C, 36.32; H, 3.04; N, 12.03; Cl, 22.85. IR, selected bands, cm^{-1}: 234 (s), 284 (vs), 335 (vs), 429 (s), 442 (sh, m), 486 (sh, w), 503 (sh, m), 664 (vs), 567 (w), 740 (vs), 751 (vs), 836 (s), 856 (s), 967 (s), 1000 (s), 1087 (vs), 1242 (vs), 1355 (vs), 1509 (s), 1627 (vs), 3230 (sh, s), 3307 (vs, br), 3500 (sh, vs). X-ray diffraction quality single crystals of complex **2** were selected directly from the reaction vessel.

[Ru$_2^{III}$(μ-Cl)$_2$Cl$_4$(Hind)$_4$]·2(Me)$_2$CO (3). A solution of **2** (0.07 g, 0.15 mmol) in acetone (10 mL) was allowed to stand at room temperature. The solution slowly turned green, and dark-red crystals were filtered off after 4 days, washed with acetone, and dried in vacuo at room temperature. Yield: 0.06 g, 79%. Anal. Calcd for C$_{34}$H$_{36}$Cl$_6$N$_8$O$_2$Ru$_2$ (M_r = 1003.58 g/mol): C, 40.69; H, 3.61; N, 11.16; Cl, 21.20. Found: C, 40.59; H, 3.59; N, 11.06; Cl, 21.03. ESI-MS in acetone (negative): *m/z* 923 [M + Cl]$^-$. IR, selected bands, cm^{-1}: 259 (s), 278 (s), 330 (vs), 343 (sh, m), 431 (m), 482 (m, b), 658 (m), 749 (vs), 965 (m), 1001 (m), 1085 (s), 1239 (s), 1356 (vs), 1510 (m), 1627 (s), 1642 (sh, w), 1709 (m), 3306 (vs, br), 3400 sh. X-ray diffraction structure and magnetic properties of this compound will be reported separately.[19]

***mer,trans*-[Ru^{III}Cl$_3$(Hind)$_2$(MeOH)] (4).** Complex **2** (0.10 g, 0.22 mmol) was dissolved in dry MeOH (8 mL) using an ultrasonic bath at room temperature for 10 min. Slow evaporation of the solvent at room temperature afforded red crystals of the product within several hours, which were filtered off, washed with diethyl ether, and dried in vacuo at room temperature. Yield: 0.06 g, 58%. Anal. Calcd for C$_{15}$H$_{16}$Cl$_3$N$_4$ORu (M_r = 475.74 g/mol): C, 37.87; H, 3.39; N, 11.78; Cl, 22.36. Found: C, 37.80; H, 3.08; N, 11.56; Cl, 22.06. ESI-MS (negative) in MeOH: *m/z* 476 [M − H]$^-$, 443 [M − MeOH − H]$^-$, 326 [RuCl$_3$(Hind) − H]$^-$. IR (KBr), selected bands, cm^{-1}: 433 (m), 660 (vs), 750 (vs), 1002 (s), 1086 (vs), 1242 (s), 1356 (s), 1509 (s), 1627 (vs), 3352 (sh, vs), 3510 (sh, m). X-ray diffraction quality single crystals of **4**·MeOH were obtained directly from the reaction vessel.

***mer,trans*-[Ru^{III}Cl$_3$(Hind)$_2$(Me$_2$S)] (5).** Dimethyl sulfide (15 μL, 0.11 mmol) was added to a solution of **2** (0.050 g, 0.11 mmol) in dry ethanol (3 mL). The resulting mixture was stirred for 5 min and allowed to stand at room temperature overnight. The orange-brown crystals were filtered off, washed with ethanol, diethyl ether, and dried in vacuo at room temperature. Yield: 0.035 g, 64%. This compound has been previously synthesized starting from **1** and fully characterized as described elsewhere.[17]

***mer,trans*-[Ru^{III}Cl$_3$(Hind)(HN=C(Me)ind)] (8a).** A solution of **2** (0.05 g, 0.11 mmol) in acetonitrile (3 mL) was allowed to stir at room temperature for 1 h. The solvent was evaporated to about 0.5 mL, and the violet solid formed was filtered off, washed with a small amount of acetonitrile, diethyl ether, and dried in vacuo at room temperature. Yield: 0.035 g, 67%. Anal. Calcd for C$_{16}$H$_{15}$Cl$_3$N$_5$Ru (M_r = 484.75 g/mol): C, 39.64; H, 3.12; N, 14.45; Cl, 21.94. Found: C, 39.42; H, 3.04; N, 14.17; Cl, 22.07. ESI-MS in MeOH (positive): *m/z*. 509 [M + Na]$^+$; 449 [M − Cl]$^+$. ESI-MS in MeOH (negative): *m/z*. 521 [M + Cl]$^-$. IR, selected bands, cm^{-1}: 277 (sh), 297 (s), 336 (s), 581 (m), 674 (m), 769 (vs), 1048 (vs), 1116 (vs), 1266 (m), 1349 (s), 1402 (m), 1471 (s), 1578 (m), 1616 (vs), 1629 (sh, m), 3278 (s), 3342 (s). X-ray diffraction quality single crystals were obtained by vapor diffusion of diethyl ether into a THF solution of **8a** to yield **8a**·Et$_2$O.

***mer,trans*-[Ru^{III}Cl$_3$(Hind)(HN=C(Ph)ind)]·PhCN (8b).** Complex **2** (0.07 g, 0.15 mmol) was dissolved in benzonitrile (3 mL) using an ultrasonic bath for 10 min, and the solution was allowed to stand at room temperature for 48 h. The red crystals were filtered off, washed with a small amount of acetone, diethyl ether, and dried in vacuo at room temperature. Yield: 0.05 g, 51%. Anal. Calcd for C$_{28}$H$_{22}$Cl$_3$N$_6$Ru (M_r = 649.94 g/mol): C, 51.74; H, 3.41; N, 12.93; Cl, 16.36. Found: C, 51.58; H, 3.48; N, 12.80; Cl, 16.27. ESI-MS in MeOH (positive): *m/z* 569 [M + Na]$^+$, 511 [M − Cl]$^+$. IR (KBr), selected bands, cm^{-1}: 665 (m), 708 (s), 756 (vs), 774 (vs), 1043 (s), 1092 (m), 1105 (m), 1116 (m), 1239 (s), 1277 (s), 1353 (s), 357 (s), 1442 (vs), 1451 (vs), 1593 (s), 1614 (vs), 1627 (sh, m), 2228 (m), 3312 (sh, s), 3220 (sh, s). X-ray diffraction quality single crystals of **8b**·PhCN were obtained from saturated solutions of **2** or **1a** in benzonitrile at room temperature.

***trans,trans*-[Ru^{III}Cl$_2$(HN=C(Me)ind)$_2$]Cl (9).** A solution of **8a** (0.07 g, 0.14 mmol) in MeCN (20 mL) was heated at 50 °C under stirring for 5 days. The solution changed from red to orange. The orange solid was isolated by centrifugation, washed with cold acetonitrile, diethyl ether, and dried in vacuo at room temperature. Yield: 0.03 g, 23%. Anal. Calcd for C$_{18}$H$_{18}$Cl$_3$N$_6$Ru (M_r = 525.80 g/mol): C, 41.12; H, 3.45; N, 15.98; Cl, 20.22. Found: C, 41.02; H, 3.22; N, 15.70; Cl, 19.95. ESI-MS (positive) in MeOH: *m/z* 490 [M]$^+$. IR (KBr), selected bands cm^{-1}: 667 (s), 746 (vs), 913 (m), 1037 (vs), 1616 (vs, br), 1628 (sh, m), 3161 (m) and 3267 (m). X-ray diffraction quality single crystals of **9**·MeCN were obtained from diluted solutions of **2** or **1a** in acetonitrile at room temperature.

***mer,trans*-[Ru^{III}Cl$_3$(Hind)$_2$(κ^{N3}-6-me$_2$ade)] (11).** *N6,N6*-Dimethyladenine (0.020 g, 0.13 mmol) was added to a solution of **2** (0.050 g, 0.11 mmol) in ethanol (15 mL), and the reaction mixture stirred at 37 °C for 48 h. The color of the solution changed from orange to green, and after about 20 h a brownish green precipitate was filtered off, washed with ethanol, and dried in vacuo. The crude product was extracted into chloroform/methanol (10:1) and precipitated with diethyl ether. The pure solid was filtered off and dried in vacuo at room temperature. Yield: 0.04 g, 62%. Anal. Calcd for C$_{21}$H$_{21}$N$_9$Cl$_3$Ru (M_r = 606.88 g/mol): C, 41.56; H, 3.48; N, 20.77; Cl, 17.53. Found: C, 41.71; H, 3.72; N, 21.08; Cl, 17.13. IR, selected bands, cm^{-1}: 284 (m), 330 (s), 753 (s), 1084 (s), 1137 (m), 1241 (m), 1356 (s), 1398 (s), 1609 (vs), 1617 (sh, m), 3260 (sh, m) and 3308 (s). ESI-MS (positive) in acetone: *m/z* 605 [M + H]$^+$. ESI-MS (negative) in acetone: *m/z* 641 [M + Cl]$^-$. X-ray

(18) Reisner, E.; Arion, V. B.; Rufińska, A.; Chiorescu, I.; Schmid, W. F.; Keppler, B. K. *Dalton Trans.* **2005**, 2355–2364.
(19) Arion, V. B.; Chibotaru, L. F. ; Cebrián-Losantos, B. , manuscript in preparation.

Table 1. Crystal Data and Details of Data Collection for **2**, **4**·MeOH and **8a**·Et_2O

complex	**2**	**4**·MeOH	**8a**·Et_2O
empirical formula	$C_{14}H_{14}Cl_3N_4ORu$	$C_{16}H_{20}Cl_3N_4O_2Ru$	$C_{20}H_{25}Cl_3N_5ORu$
fw	461.71	507.78	558.87
space group	*Cc*	$P2_1/c$	*C*2/*c*
a, Å	23.2227(13)	8.1718(3)	21.2476(8)
b, Å	24.8073(13)	12.0086(5)	13.0596(8)
c, Å	8.6427(5)	21.2128(8)	16.8248(6)
β, deg	94.679(6)	99.626(3)	96.347(4)
V, Å^3	4962.4(5)	2052.34(14)	4640.0(4)
Z	12	4	8
ρ_{calcd}, g cm^{-3}	1.854	1.643	1.600
crystal size, mm^3	0.20 × 0.20 × 0.10	0.26 × 0.12 × 0.12	0.26 × 0.03 × 0.03
T, K	100	296	100
μ, cm^{-1}	14.40	11.72	10.43
*R*1[a]	0.0483	0.0371	0.0256
*wR*2[b]	0.1250	0.0970	0.0598
GOF[c]	1.064	1.054	1.013

[a] $R1 = \Sigma||F_o| - |F_c||/\Sigma|F_o|$. [b] $wR2 = \{\Sigma[w\,(F_o^2 - F_c^2)^2]/\Sigma[w(F_o^2)^2\,]\}^{1/2}$. [c] GOF $= \{\Sigma[w(F_o^2 - F_c^2)^2]/(n - p)\}^{1/2}$, where *n* is the number of reflections and *p* is the total number of parameters refined.

Table 2. Crystal Data and Details of Data Collection for **8b**·PhCN, **9**·MeCN, **11**·THF and **12**

complex	**8b**·PhCN	**9**·MeCN	**11**·THF	**12**
empirical formula	$C_{28}H_{22}Cl_3N_6Ru$	$C_{20}H_{21}Cl_3N_7Ru$	$C_{26}H_{29}Cl_3N_9ORu$	$C_{22}H_{28}Cl_4N_4NaO_4Ru$
fw	649.94	566.86	678.99	678.34
space group	$P\bar{1}$	$P\bar{1}$	$P\bar{1}$	$P\bar{1}$
a, Å	9.808(2)	9.1416(8)	10.690(2)	6.5950(4)
b, Å	11.927(2)	10.5096(7)	12.757(3)	7.7044(4)
c, Å	12.689(3)	13.0426(12)	12.957(3)	14.1038(8)
α, deg	104.96(3)	102.157(6)	116.63(3)	75.446(3)
β, deg	107.96(3)	106.752(7)	103.45(3)	83.563(4)
γ, deg	93.78(3)	95.512(6)	103.08(3)	84.134(3)
V, Å^3	1347.0(5)	1156.41(17)	1420.8(5)	687.21(7)
Z	2	2	2	1
ρ_{calcd}, g cm^{-3}	1.602	1.628	1.587	1.639
crystal size, mm^3	0.08 × 0.06 × 0.04	0.20 × 0.06 × 0.01	0.20 × 0.17 × 0.06	0.10 × 0.10 × 0.05
T, K	100	100	120	100
μ, cm^{-1}	9.10	10.47	8.71	10.11
*R*1[a]	0.0331	0.0370	0.0286	0.0303
*wR*2[b]	0.0626	0.0852	0.0816	0.0893
GOF[c]	1.062	1.006	1.023	1.095

[a] $R1 = \Sigma||F_o| - |F_c||/\Sigma|F_o|$. [b] $wR2 = \{\Sigma[w\,(F_o^2 - F_c^2)^2]/\Sigma[w(F_o^2)^2\,]\}^{1/2}$. [c] GOF $= \{\Sigma[w(F_o^2 - F_c^2)^2]/(n - p)\}^{1/2}$, where *n* is the number of reflections and *p* is the total number of parameters refined.

diffraction quality crystals of **11**·THF were grown by vapor diffusion of *n*-hexane into a saturated THF solution of complex **11**.

Physical measurements. Elemental analyses were carried out at the Microanalytical Service of the Institute of Physical Chemistry of the University of Vienna and were within ±0.4% of the theoretical values. Infrared spectra were obtained from KBr (4000—400 cm^{-1}) or CsI (400—200 cm^{-1}) pellets with a Perkin-Elmer FT-IR 2000 instrument. UV—vis spectra were recorded on a Perkin-Elmer Lambda 20 UV—vis spectrophotometer. Electrospray ionization mass spectrometry was carried out with a Bruker Esquire 3000 instrument (Bruker Daltonic, Bremen, Germany). Expected and experimental isotope distributions were compared. ^{1}H NMR spectra were recorded at 400.13 MHz on a Bruker DPX400 (Ultrashield Magnet) spectrometer. Conductivity measurements were performed by using a Meter LF 538 (Weinheim, Germany).

Crystallographic Structure Determination. X-ray diffraction measurements were performed on a Bruker X8APEXII or Nonius Kappa CCD diffractometers with graphite-monochromated Mo Kα radiation (λ = 0.71073 Å), controlled by a Pentium-based PC running the SAINT or Denzo-SMN software package.[20] Single crystals were positioned at 40, 40, 37.5, 37.5, 40, 30, and 40 mm from the detector and 1367, 1262, 1250, 957, 1027, 337, and 1963 frames were measured, each for 50, 30, 60, 90, 80, 65, and 50 s over 1, 1, 1, 1, 1, 2 and 1° scan for **2**, **4**·MeOH, **8a**·Et_2O, **8b**·PhCN, **9**·MeCN, **11**·THF, and **12**, correspondingly. Crystal data, data collection parameters, and structure refinement details for **2**, **4**, and **8a** are given in Table 1 and for **8b**, **9**, **11**, and **12** in Table 2. The structures were solved by direct methods and refined on F^2 by full-matrix least-squares techniques using the SHELXTL software package.[21–23] All non-hydrogen atoms were refined with anisotropic displacement parameters. Hydrogen atoms were placed at calculated positions or localized on difference Fourier maps and isotropically refined. Calculated hydrogen atoms have assigned thermal parameters equal to either 1.5 (methyl hydrogen atoms) or 1.2 (nonmethyl hydrogen atoms) times the thermal parameters of the atom to which they were attached. The graphics were prepared by using the Oak Ridge Thermal Ellipsoid Plot (ORTEP).[24]

(20) (a) *SAINT-Plus, version 7.06a and APEX2*; Bruker-Nonius AXS Inc.: Madison, WI, 2004. (b) Otwinowski, Z.; Minor, W. In *Methods in Enzymology.*; Carter, C. W., Jr. , Sweet, R. M., Eds.; Academic Press: New York, 1997; Macromolecular Crystallography, part A, Vol. *276*, pp 307—326.
(21) Sheldrick, G. M. *SHELXS-97, Program for Crystal Structure Solution*; University Göttingen: Göttingen, Germany, 1997.
(22) Sheldrick, G. M. *SHELXL-97, Program for Crystal Structure Refinement*; University Göttingen: Göttingen, Germany, 1997.
(23) *International Tables for X-ray Crystallography*; Kluwer Academic Press: Dodrecht, The Netherlands, 1992; Vol. *C*, Tables 4.2.6.8 and 6.1.1.4.
(24) Johnson, G. K. *Report ORNL-5138*; Oak Ridge National Laboratory: Oak Ridge, TN, 1976.

Scheme 1. Synthetic Routes to Complexes **2**−**12**

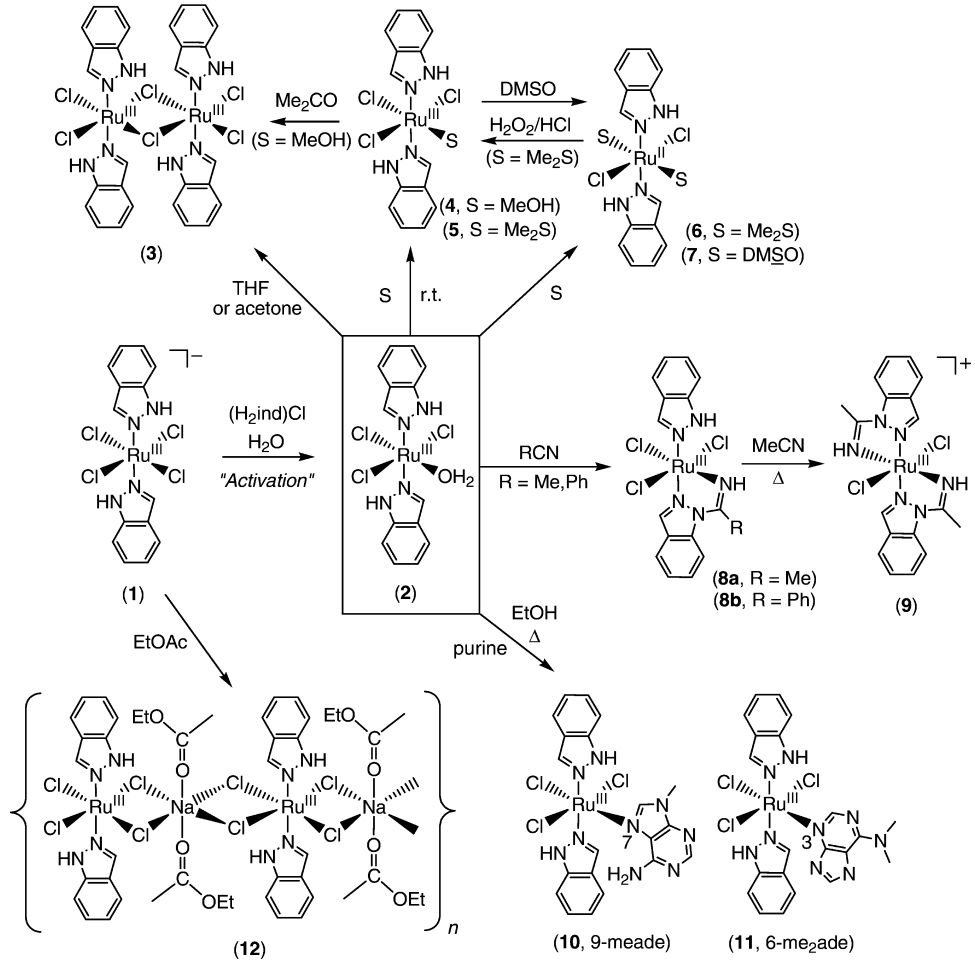

Electrochemistry. Cyclic voltammograms (CVs) were measured in a three-electrode cell using a 2 mm-diameter platinum-disk or glassy carbon working electrode, a platinum auxiliary electrode, and a Ag|Ag$^+$ reference electrode containing 0.1 M $AgNO_3$, the potential of which was corrected using an internal standard redox couple of ferrocenium/ferrocene. Measurements were performed using an EG&G PARC 273A potentiostat/galvanostat. Deaeration of solutions was accomplished by passing a stream of argon through the solution for 5 min prior to the measurement and then maintaining a blanket atmosphere of argon over the solution during the measurement. The potentials were measured in 0.20 M [*n*-Bu_4N][BF_4]/DMF or DMSO, using [Fe(η^5-C_5H_5)$_2$] ($E_{1/2}$ = +0.72 V or +0.68 V vs NHE, respectively)[25] as internal standard, and are quoted relative to NHE. For digital simulations (kinetic studies) the Electrochemical Simulation Package (ESP, version 2.4) from C. Nervi, (nervi@lem.ch.unito.it, Dipartimento di Chimica IFM: Torino, Italy, 1994/98) was used. The electrolyte solutions for low temperature measurements (±2 °C) were externally cooled with $CaCl_2 \cdot 6H_2O$/ice.

Results and Discussion

Synthesis, Reactivity of *mer*,*trans*-[RuCl$_3$(Hind)$_2$(H$_2$O)] (2) and Spectroscopic Characterization. The synthetic routes to complexes **2**−**12** are depicted in Scheme 1. Complex **2** was isolated as red crystals in 85% yield from an aqueous solution of Na[*trans*-Ru^{III}Cl$_4$(Hind)$_2$]·1.5H$_2$O (**1a**) and indazolium chloride in 1:1.1 molar ratio at room temperature after 48 h. Although the aquation behavior of NAMI-A and KP1019 has been investigated intensively,[7,26] their monoaqua analogues have been previously reported only for related complexes, viz., *mer*-[RuCl$_3$(dmtp)$_2$(*S*-DMSO)(H$_2$O)] (dmtp = 5,7-dimethyl-1,2,4-triazolo[1,5-a]pyrimidine),[27] *mer*-[RuCl$_3$(1-methylindazole)$_2$(H$_2$O)],[28] and *mer*-[RuCl$_3$(dmtp)$_2$(H$_2$O)].[29] Complex **2** is insoluble in water but is soluble in various organic solvents. The solution of **2** in THF or acetone generates dark-red crystals of a dinuclear ruthenium(III) species (**3**) with two μ-chlorido bridges in 79% yield (from acetone solution) after several days. Using stronger donor solvents, for example, MeOH, or stronger

(25) Barette, W. C. J.; Johnson, H. W. J.; Sawyer, D. T. *Anal. Chem.* **1984**, *56*, 1890–1898.

(26) (a) Bacac, M.; Hotze, A. C. G.; van der Schilden, K.; Haasnoot, J. G.; Pacor, S.; Alessio, E.; Sava, G.; Reedijk, J. *J. Inorg. Biochem.* **2004**, *98*, 402–412. (b) Sava, G.; Bergamo, A.; Zorzet, S.; Gava, B.; Casarsa, C.; Coccietto, M.; Furlani, A.; Scarcia, V.; Serli, B.; Iengo, E.; Alessio, E.; Mestroni, G. *Eur. J. Cancer* **2002**, *38*, 427–435. (c) Groessl, M.; Reisner, E.; Hartinger, C. G.; Eichinger, R.; Semenova, O.; Timerbaev, A. R.; Jakupec, M. A.; Arion, V. B.; Keppler, B. K. *J. Med. Chem.* **2007**, *50*, 2185–2193.

(27) Velders, A. H.; Bergamo, A.; Alessio, E.; Zangrando, E.; Haasnoot, E.; Casarsa, J. G.; Cocchietto, M.; Zorzet, S.; Sava, G. *J. Med. Chem.* **2004**, *47*, 1110–1121.

(28) Lipponer, K. G.; Vogel, E.; Keppler, B. K. *Met.-Based Drugs* **1996**, *3*, 243–260.

(29) Velders, A. H.; Pazderski, L.; Ugozzoli, F.; Bianini-Cingi, M.; Manotti-Lanfredi, A. M.; Haasnoot, J. G.; Reedijk, J. *Inorg. Chim. Acta* **1998**, *273*, 259–265.

coordinating ligands, for example, dialkyl thioether, the aqua ligand in **2** was replaced at room temperature to yield *mer,trans*-[$Ru^{III}Cl_3$(Hind)$_2$(MeOH)] (**4**) and *mer,trans*-[$Ru^{III}Cl_3$(Hind)$_2$(Me_2S)] (**5**). Complex **3** can also be prepared by dissolution of **4** in acetone. As previously reported for **1**,[17,18] *trans,trans,trans*-[$Ru^{II}Cl_2$(Hind)$_2$(Me_2S)$_2$] (**6**) and *trans, trans,trans*-[$Ru^{II}Cl_2$(Hind)$_2$(*S*-DMSO)$_2$] (**7**) were prepared from **2** with an excess of Me_2S or DMSO, respectively. Replacement of one aqua and one chlorido ligand in *trans*-positions to each other was accompanied by reduction of ruthenium(III) to ruthenium(II). Oxidation of **6** with hydrogen peroxide/12 M HCl leads to substitution of one of the two dialkyl sulfide ligands by a chloride ion and formation of **5** as described previously.[17]

Solvolysis of **2** in RCN at room temperature afforded *mer,trans*-[$Ru^{III}Cl_3$(Hind)(HN=C(R)ind)] [R = Me (**8a**) or Ph (**8b**)] via the insertion of the C≡N group of the nitrile into the N1—H bond of the N2-coordinated indazole. Metal-mediated iminoacylation of nitriles is well documented[30–34] but has not been observed so far for ruthenium(III) as the activating Lewis acid. Amidines are interesting with respect to organic,[35] medicinal,[36] and coordination chemistry.[37] The ruthenium(III)-assisted iminoacylation of indazole reported herein is unprecedented and proceeds much faster (within seconds at room temperature for **8a**) than reported previously for ruthenium(II). In particular, *trans,cis*-[$Ru^{II}Cl_2$(*S*-DMSO)$_2$(HN=C(R)ind)] was produced from a solution of *trans,cis,cis*-[$Ru^{II}Cl_2$(*S*-DMSO)$_2$(Hind)$_2$] in acetonitrile only within days.[18] It was speculated that the Ru(II) mediated iminoacylation is stimulated by strong π-accepting properties of *trans*-standing ligands, for example, DMSO[18] in *trans, cis,cis*- and *trans,trans,trans*-[$Ru^{II}Cl_2$(*S*-DMSO)$_2$(Hind)$_2$] or CO[30] in [RuH(CO)(RCN)$_2$(PPh_3)$_2$]$^+$. Complex **2** does not contain such activating *trans*-ligands, but the higher metal oxidation state allows for sufficient activation of the coordinated indazole. Higher metal oxidation states significantly enhance the activation of coordinated nitriles.[30] Thus, coordinated RCN is activated up to 3 orders of magnitude when bound to platinum(IV) versus platinum(II).[38]

The first reaction step presumably involves replacement of the water ligand by acetonitrile resulting in the activation of the nitrile molecule upon formation of the [$Ru^{III}Cl_3$(Hind)$_2$(RCN)] intermediate (Supporting Information, Scheme S1). This hypothesis is supported by the lability of the aqua ligand and the formation of complexes **3**—**5** via quick release/substitution of the coordinated water molecule(s). In addition, the formation of [$Ru^{III}Cl_3$(Hind)$_2$(RCN)] as an intermediate is suggested when monitoring the reaction of **2** in MeCN by cyclic voltammetry at lower temperatures (see below). By prolonged heating of **2** in MeCN, *trans*-[$Ru^{III}Cl_2$(HN=C(Me)ind)$_2$]Cl (**9**) with two cyclic amidine ligands was isolated. Complex **9** is the first example of a metal complex with two amidine ligands resulting from iminoacylation of coordinated azole ligands.

Table 3. Charge Transfer Bands for Complexes **1**—**6** and **8**—**11**

complex (solvent)	λ_1/nm (ε_1/mM^{-1} cm^{-1})	λ_2/nm (ε_2/mM^{-1} cm^{-1})
1 (H_2O)	377 (6.0)	444[b] (3.5)
2 (DMF)	355 (6.1)	417 (1.4)
3 (THF)	358[b] (6.6)	429 (4.4)
4 (MeOH)	354[b] (4.4)	409 (1.8)
5[a] ($CHCl_3$)	366 (3.8)	444 (1.9)
6[a] ($CHCl_3$)	361 (12.6)	
8a (MeCN)	375 (6.0)	431[b] (1.5)
8b (DMF)	389 (1.1)	465[b] (2.6)
9 (MeCN)	374 (9.3)	448[b] (2.0)
10[a] (MeOH)	380 (3.3)	428 (2.0)
11 (MeOH)	379 (4.7)	433 (2.4)

[a] From ref 17. [b] Shoulder.

Complexes **10** and **11** were synthesized by reaction of **2** with 9-meade or 6-me_2ade, respectively, in MeOH or EtOH upon heating. Both complexes can also be prepared starting from **1** under similar experimental conditions but markedly longer reaction times. Coordination of the purine base takes place via N7 in **10**,[17] whereas it occurs through N3 in **11**. Therefore, N3 can be considered as an alternative to the N7 purine base binding site for the Ru(III) center. The X-ray structure of **11** is the first crystallographic evidence for monofunctional binding via N3 of *N6,N6*-dimethyladenine to ruthenium. Coordination via the more basic N1 site (compared to N3) is presumably precluded by the bulky $N(Me)_2$ group.

Characteristic charge transfer absorption bands for complexes **1**—**6** and **8**—**11** are summarized in Table 3 (for additional UV—vis data see Supporting Information). Spectroscopic investigations of **7** in solution were hampered by its low solubility in organic solvents. The presence of coordinated water in **2** is confirmed by IR spectroscopy with a broad band around 3500 cm^{-1}. Molar conductivity of **2** was determined in DMSO at 1.88 S cm^2 mol^{-1} indicating the presence of a neutral species and no change was observed over several hours. The IR spectra of complexes **1**—**7** show stretching vibrations for ν(*C*=N, indazole) at 1627 ± 3 cm^{-1}. The presence of a second vibration at 1615 ± 2 cm^{-1} in the spectra of **8a**, **8b**, and **9** can be tentatively attributed to ν(*C*=N, HN=C(R)). This stretching frequency for the amidine is lower than previously reported for ruthenium(II) compounds, for example, [Ru^{II}(CO)(CH=CHPh)-{HN=C(Me)(Me_2pz)}(PPh_3)$_2$]PF_6 (ν = 1628 cm^{-1}),[30] [(η^4-C_8H_{12})$_2$$Ru^{II}_2$H{$\mu$-*N*=C(Me)pz}($\mu$-pz)($\mu$-H)] ($\nu$ = 1653 cm^{-1}),[31] and *trans*-[$Ru^{II}Cl_2$(*S*-DMSO)(Hind){HN=C(Me)ind}] (ν = 1643 cm^{-1}),[18] but is presumably indicative for the stronger activation at the Ru(III) center compared to Ru(II).

We investigated the potentially higher reactivity of the aquated species **2** compared to **1**. Preliminary qualitative

(30) Kukushkin, V.Yu.; Pombeiro, A. J. L. *Chem. Rev.* **2002**, *102*, 1771–1802; and references therein.
(31) Albers, M. O.; Crosby, S. F. A.; Liles, D. C.; Robinson, D. J.; Shaker, A.; Singleton, E. *Organometallics* **1987**, *6*, 2014–2017.
(32) López, J.; Santos, A.; Romero, A. *J. Organomet. Chem.* **1993**, *443*, 221–228.
(33) Arroyo, M.; Miguel, D.; Villafane Nieto, S.; Pérez, J.; Riera, L. *Inorg. Chem.* **2006**, *45*, 7018–7026.
(34) Khripun, A. V.; Kukushkin, V. Yu.; Selivanov, S. I.; Haukka, M.; Pombeiro, A. J. L. *Inorg. Chem.* **2006**, *45*, 5073–5083.
(35) Raczynska, E. D.; Gawinecki, R. *Trends Org. Chem.* **1998**, *7*, 85–93.
(36) (a) Greenhill, J. V.; Lue, P. *Prog. Med. Chem.* **1993**, *30*, 203–326. (b) Richter, P. H.; Wunderlich, L.; Schleuder, H.; Keckeis, A. *Pharmazie* **1993**, *48*, 163–184.
(37) Barker, J.; Kilner, M. *Coord. Chem. Rev.* **1994**, *133*, 219–300.

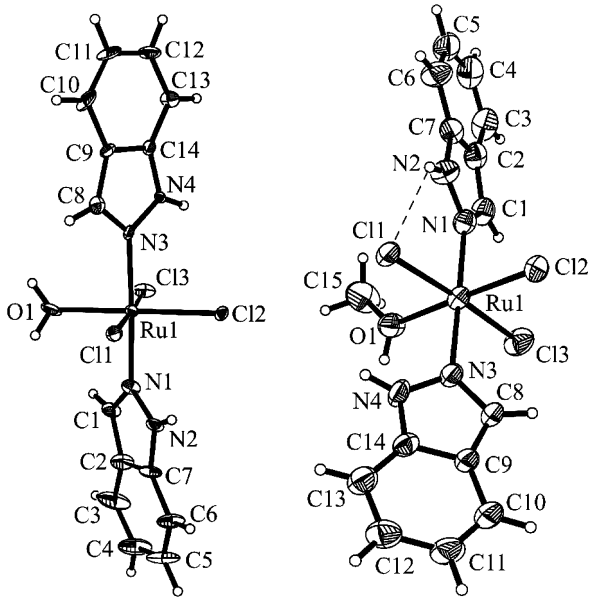

Figure 2. Structure of the first independent molecule of **2** (left) and of molecule **4** (right) with thermal ellipsoids drawn at 50% (**2**) and 30% probability level (**4**), respectively.

studies show that the Ru^{III}—OH$_2$ bond is indeed more labile than the Ru^{III}—Cl bond.[39,40] The release or substitution of the aqua ligand in **2** and subsequent dimerization is indicative of the labile nature of the H$_2$O ligand. No such reaction was ever observed for **1**. Complex **4** was formed immediately after dissolution of **2** in MeOH at room temperature, whereas it took several hours until **4** was generated in methanolic solutions of **1** as monitored by UV−vis spectroscopy. Complex **2** reacts quantitatively within seconds in MeCN to give **8a** as detected by spectroscopic and electrochemical techniques (see below), whereas **1** is stable in the same solvent within days.[7b] Interestingly, **1** was shown to react readily in aqueous MeCN to form one main solvent species, presumably as a result of aquation to **2** and replacement of the aqua ligand by MeCN.[7b] Formation of complex **5** upon replacement of H$_2$O or Cl$^-$ by Me$_2$S in acetone at room temperature occurs within 1−2 h for **2**, whereas only about 50% converted into the product after several days when using **1** as the starting material. NMR measurements show that **2** reacts faster with 9-meade than **1**, and quantitative kinetic studies are underway in our laboratory.

Structural Characterization. Complex **2** (Figure 2) crystallizes in the monoclinic space group *Cc* with three independent molecules of **2** per asymmetric unit. Two indazole ligands are in the axial positions, and three chlorido ligands and one water molecule occupy the equatorial plane of the distorted octahedron. The average Ru—Cl bond length in **2** of 2.333(4) Å is similar to those found in *mer,trans*-[Ru^{III}Cl$_3$(1-methylindazole)$_2$(H$_2$O)][28] at 2.339(18) Å and slightly shorter than in (Ph$_4$P)[*trans*-Ru^{III}Cl$_4$(Hind)$_2$][14] at 2.3639(17) Å. The average Ru—O bond length in **2** at 2.076(10) Å for the three crystallographically independent molecules is similar to that found in *mer,trans*-[Ru^{III}Cl$_3$(1-methylindazole)$_2$(H$_2$O)] and in *mer,trans*-[Ru^{III}Cl$_3$-(dmtp)$_2$(H$_2$O)]·H$_2$O[29] at 2.109(17) and 2.101(4) Å, respectively. The average Ru—N bond in **2** at 2.056(4) Å is well comparable with those in (Ph$_4$P)[*trans*-Ru^{III}Cl$_4$(Hind)$_2$] [2.052(21) and 2.071(22) Å]. The crystal structure is stabilized by intermolecular H-bonding interactions between the three independent molecules of *mer,trans*-[Ru^{III}Cl$_3$(Hind)$_2$-(H$_2$O)]: N12−H···Cl5 [N12−H 0.880, H···Cl5 2.401, N12···Cl5 3.218 Å, ∠N12HCl5 154.50°], N6—H···Cl8 [N6−H 0.880, H···Cl8 2.378, N6···Cl8 3.177 Å, ∠N6HCl8 151.18°], N6—H···Cl4 [N6−H 0.880, H···Cl4 2.716, N6···Cl4 3.133 Å, ∠N6HCl4 110.37°], O1−H···Cl4 [O1−H 0.860, H···Cl4 2.370, O1···Cl4 3.150 Å, ∠O1HCl4 151.00°], O2—H···Cl6 [O2−H 0.861, H···Cl6 2.645, O2···Cl6 3.072 Å, ∠O2HCl6 111.88°], and O2—H···N2 [O2−H 0.861, H···N2 2.452, O2···N2 3.287 Å, ∠O2HN2 163.89°]. Other intermolecular hydrogen bonds are quoted in Supporting Information, Table S1.

Complex **4**·MeOH (Figure 2) crystallizes in the monoclinic space group $P2_1/c$. The asymmetric unit consists of one molecule of complex **4** and one molecule of methanol. The ruthenium(III) ion in **4** has the expected distorted octahedral coordination geometry, with three meridional chlorido ligands, and a methanol molecule in the equatorial positions and two indazole ligands in the axial positions. The Ru−O distance to the coordinated methanol molecule of 2.056(3) Å is slightly shorter than those found in complex **2** (see above), *mer*-[RuCl$_3$(acv)(*S*-DMSO)(CH$_3$OH)]·0.5CH$_3$-OH (acv = acyclovir)[41] [2.072(6) Å] and [Ru^{III}Cl$_3$(bpy)(CH$_3$OH)]·CH$_3$OH [2.118(7) Å].[42] The Ru—N1 and Ru—N3 distances at 2.085(4) and 2.053(4) Å, respectively, with an N3—Ru—N1 angle of 177.93(15)° and the average Ru—Cl bond length at 2.331(12) Å are normal for ruthenium(III) chlorido compounds.

The crystal structures of **8a**·Et$_2$O and **8b**·PhCN consist of neutral molecules of [Ru^{III}Cl$_3$(Hind){HN=C(R)ind}], where R = Me or Ph (Figure 3) and molecules of Et$_2$O and PhCN, correspondingly. The Ru atom in both compounds is coordinated axially by two chlorido ligands [Ru—Cl1 2.3358(7) and Ru—Cl3 2.3555(7) Å (**8a**), Ru—Cl1 2.3467(11) and Ru—Cl3 2.3095(11) Å (**8b**)] and equatorially by three different ligands: a chlorido ligand [Ru—Cl2 2.3680(6) and 2.3647(8) Å in **8a** and **8b**, respectively), indazole [Ru—N4 2.077(2) (**8a**) and 2.059(2) Å (**8b**)] and a bidentate ligand formed via coupling of acetonitrile or benzonitrile with indazole. Chelation of the Ru center by the corresponding amidine ligand is reflected in the Ru—N2 and Ru—N3 distances of 2.0228(19) and 2.0190(19) (**8a**), and 2.026(2) and 2.036(2) Å (**8b**) compared to 2.0363(16) and 2.0594(18) Å for such bonds in [Ru^{II}Cl$_2$(*S*-DMSO)(Hind){HN=C(Me)ind}].[18] The bite angle N2—Ru—N3 of 78.11(8) and 77.77(9)° in **8a** and **8b**, respectively, is comparable to that

(38) Luzyanin, K. V.; Kukushkin, V.Yu.; Ryabov, A. D.; Haukka, M.; Pombeiro, A. J. L. *Inorg. Chem.* **2005**, *44*, 2944–2953.
(39) Zanella, A. W.; Ford, P. C. *Inorg. Chem.* **1975**, *14*, 42–47.
(40) Coleman, G. N.; Gesler, J. W.; Shirley, F. A.; Kuempel, J. R. *Inorg. Chem.* **1973**, *12*, 1036–1038.
(41) Turel, I.; Pečanac, M.; Golobič, A.; Alessio, E.; Serli, B. *Eur. J. Inorg. Chem.* **2002**, 1928–1931.
(42) Eskelinen, E.; Da Costa, P.; Haukka, M. *J. Electroanal. Chem.* **2005**, *579*, 257–265.

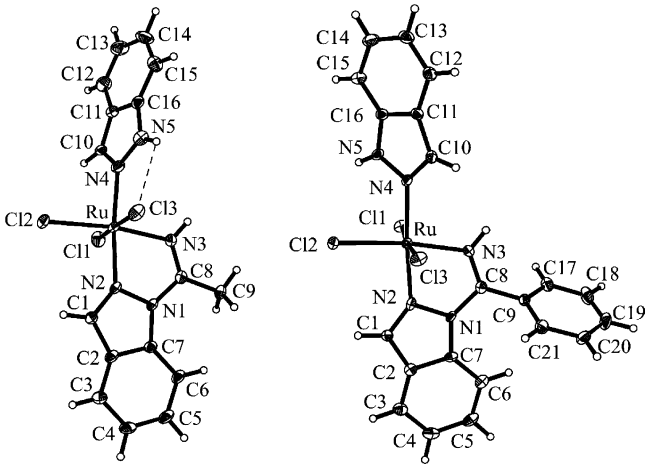

Figure 3. Molecular structures of **8a**·Et_2O (left) and **8b**·PhCN (right) with thermal ellipsoids drawn at 50% probability level. The solvent molecules have been omitted for clarity.

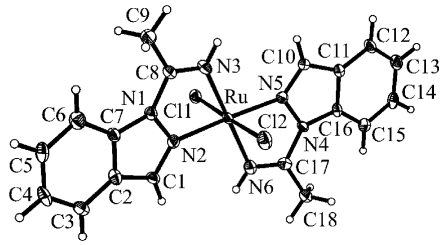

Figure 4. Structure of the cation in $[Ru^{III}Cl_2\{HN{=}C(Me)ind\}_2]Cl$·MeCN (**9**·MeCN) with thermal ellipsoids drawn at 50% probability level.

in $[Ru^{II}Cl_2(S\text{-DMSO})(Hind)\{HN{=}C(Me)ind\}]$ at 77.26(7)° and significantly larger than in the dimethylpyrazolylamidine $[Ru(CO)(CH{=}CHCMe_3)\{NH{=}C(Me)(Me_2pz)\}(PPh_3)_2]PF_6$·$CH_2Cl_2$ complex at 72.8(3)°.[32]

The crystal structure of the **9**·MeCN consists of cations $[Ru^{III}Cl_2\{HN{=}C(Me)ind\}_2]^+$, chloride anions, and molecules of acetonitrile (Figure 4). The Ru atom is coordinated axially by two chlorido ligands [Ru—Cl1 2.3509(11) and Ru—Cl2 2.2971(11) Å] and equatorially by two bidentate ligands formed via coupling of acetonitrile with indazole [Ru—N2 2.031(3), Ru—N3 2.043(3), Ru—N5 2.032(3), and Ru—N6 2.043(3) Å]. The bite angles N2—Ru—N3 at 76.98(13) and N5—Ru—N6 at 77.46(13)° are only slightly smaller than in **8a** and **8b**.

Complex **11** crystallizes in the triclinic space group $P\bar{1}$ with one independent molecule of $[Ru^{III}Cl_3(Hind)_2(\kappa^{N3}\text{-}6\text{-}me_2ade)]$ and one THF molecule in the asymmetric unit (Figure 5). The ruthenium atom is coordinated in the equatorial plane by three chlorido ligands and a nitrogen atom N3 of the ligand *N6,N6*-dimethyladenine and axially by two indazole ligands. The Ru—N13 of 2.074(2) and Ru—N22 bond of 2.068(2) Å are similar to those in *mer,trans*-$[Ru^{III}Cl_3(Hind)_2(\kappa^{N7}\text{-}9\text{-}meade)]$·$CH_2Cl_2$·$CH_3OH$ (**10**) with Ru—N21 of 2.069(2) and Ru—N12 of 2.0748(19) Å.[17] The bond lengths Ru—N3 [2.0914(19)], Ru—Cl1 [2.3401(14)], Ru—Cl2 [2.3469(14)] and Ru—Cl3 [2.3368(8) Å] in **11** are well comparable to Ru—N7 [2.1039(17)], Ru—Cl1 [2.3416(8)], Ru—Cl2 [2.3450(8)] and Ru—Cl3 [2.3315(8) Å] in complex *mer,trans*-$[Ru^{III}Cl_3(Hind)_2(\kappa^{N7}\text{-}9\text{-}meade)]$·$CH_2Cl_2$·$CH_3OH$ (**10**).[17] The structure of **11** is stabilized by five hydrogen

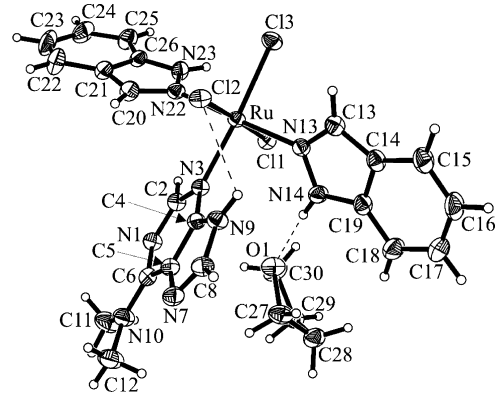

Figure 5. Fragment of the crystal structure of $[Ru^{III}Cl_3(Hind)_2(\kappa^{N3}\text{-}6\text{-}me_2ade)]$·THF (**11**·THF) with thermal ellipsoids drawn at 50% probability level showing the hydrogen bonding interactions N14—H···O1 and N9—H···Cl2.

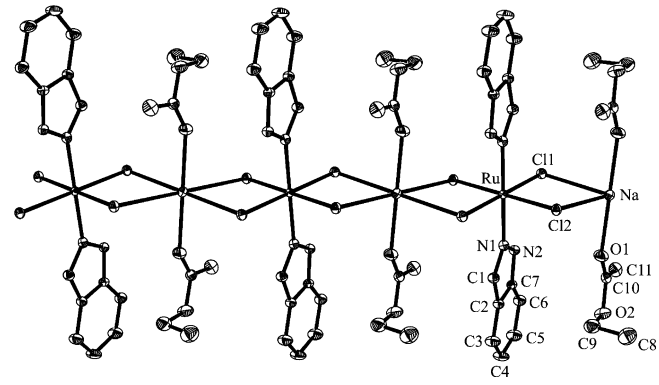

Figure 6. Fragment of the structure of $[Na(EtOAc)_2RuCl_4(Hind)_2]_n$ (**12**); thermal ellipsoids are drawn at 50% probability level. Selected bond distances (Å) and bond angles (°): Ru—N1 2.0680(19), Ru—Cl1 2.3596(6), Ru—Cl2 2.3556(5), Na—Cl1 2.7743(6), Na—Cl2 2.7967(6), Na—O1 2.3142(19), N1—Ru—N1′ 180.00, O1—Ru—O1′ 180.00.

bonding interactions, a strong one between the O1 of the solvent molecule THF and atom N14 of the coordinated indazole N14—H···O1 [N14—H 0.880, H···O1 1.876, N14···O1 2.739 Å and ∠N14HO1 166.36°] and four weaker interactions N9—H···Cl2 [N9—H 0.880, H···Cl2 2.676, N9···Cl2 3.143 Å, and ∠N9HCl2 114.36°], N9—H···Cl2′($-x + 2, -y + 1, -z + 2$) [N9—H 0.880, H···Cl2′ 2.503, N9···Cl2′ 3.216 Å, and ∠N9HCl2′ 138.55°], N23—H···Cl1″($-x + 2, -y + 1, -z + 1$) [N23—H 0.880, H···Cl1″ 2.836, N23···Cl1″ 3.387 Å, and ∠N23HCl1 122.20°], and N23—H···Cl3″ [N23—H 0.880, H···Cl3″ 2.853, N23···Cl3″ 3.536 Å, and ∠N23HCl3″ 135.59°] (Figure 5).

The crystal structure of **12** consists of octahedral {*trans*-$RuCl_4(Hind)_2$} units bridged by sodium ions in alternate fashion which results in a polymeric chain shown in Figure 6. The coordination number of the sodium cation is completed to six by two axial ethyl acetate ligands. The Ru—Cl and Ru—N bond lengths are typical for the *trans*-$[RuCl_4(Hind)_2]^-$ anion. Whereas Na—Cl bond lengths are well comparable with those in $[(C_5Me_5)_2Pr(\mu\text{-}Cl)_2Na(dimethoxyethane)_2]$ of 2.872(9) and 2.760(11) Å, the Na—O1 at 2.3142(19) Å in **12** is markedly shorter than in $[(C_5Me_5)_2Pr(\mu\text{-}Cl)_2Na(dme)_2]$ with $Na{-}O_{average} = 2.43(3)$ Å.[43]

Table 4. Cyclic Voltammetric Data for Ruthenium(III) Complexes **1**, **2**, **5**, **8a**, **8b**, **10**, and **11**

complex	experimental[a]	
	$E_{1/2}/I^{red}$	$E_{1/2}/a^b$
trans-[Ru^{III}Cl$_4$(Hind)$_2$]$^-$ (**1**)[c]	−0.43* (−0.41*)	−0.15
mer,trans-[Ru^{III}Cl$_3$(Hind)$_2$(H$_2$O)] (**2**)	−0.16 (−0.14*)	0.21 (0.67)
mer,trans-[Ru^{III}Cl$_3$(Hind)$_2$(Me$_2$S)] (**5**)[d]	0.16 (0.18)	0.51 (0.95)
mer,trans-[Ru^{III}Cl$_3$(Hind)(HN=C(Me)ind)] (**8a**)	0.01 (0.01)	0.30 (0.84)
mer,trans-[Ru^{III}Cl$_3$(Hind)(HN=C(Ph)ind)] (**8b**)	0.06 (0.06)	0.38 (0.86)
mer,trans-[Ru^{III}Cl$_3$(Hind)$_2$(κ^{N7}-9-meade)] (**10**)[d]	0.02 (0.03)	0.36 (0.93)
mer,trans-[Ru^{III}Cl$_3$(Hind)$_2$(κ^{N3}-6-me$_2$ade)] (**11**)	0.04 (0.04)	0.34 (0.92)

[a] Potentials in V ± 0.02 vs NHE measured at a scan rate of 0.20 V s^{-1}, in 0.20 M [*n*Bu$_4$N][BF$_4$]/DMF (or DMSO, in brackets). $E_{1/2}$ values are given for the reversible waves, whereas for the irreversible ones, the $E_{p/2}$ values are marked with an asterisk (*). [b] Formed after cathodically induced metal dechlorination upon Ru^{III}→Ru^{II} reduction (i.e., [M − Cl + solvent]). [c] Taken from ref 44. [d] Taken from ref 17.

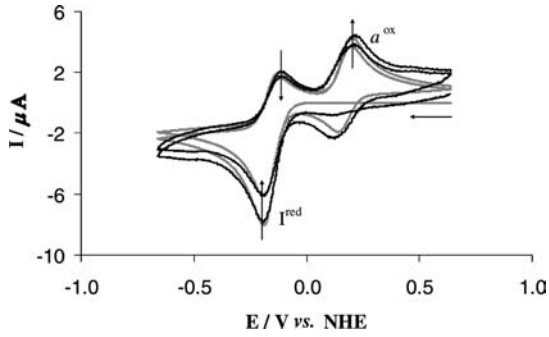

Figure 7. Experimental (2.0 mM in 0.20 M [*n*–Bu$_4$N][BF$_4$]/DMF, black line) and simulated cyclic voltammograms (gray line) for *mer,trans*-[Ru^{III}Cl$_3$(Hind)$_2$(H$_2$O)] (**2**) at a scan rate of 0.07 V s^{-1}. The simulated cyclic voltammograms were obtained by using the optimized values $k_1 = 0.24$ s^{-1} and $k_2 = 0.01$ s^{-1}.

Electrochemical Studies. The stability of all complexes was investigated by UV−vis spectroscopy in DMF and DMSO solutions prior to the electrochemical investigations. Complexes **1**, **2**, **5**, **6**, **8a**, **8b**, **10**, and **11** were sufficiently stable at room temperature for electrochemical studies, whereas chemical instability or insolubility in the electrolyte solutions prevented the measurement of complexes **3**, **4**, **7**, and **9**. The cyclic voltammograms of 0.20 M [*n*-Bu$_4$N][BF$_4$]/DMF and DMSO solutions of the ruthenium(III) complexes **1**, **2**, **5**, **8a**, **8b**, **10**, and **11** at a platinum disk or glassy carbon working electrode display one Ru^{III}→Ru^{II} reduction wave, I^{red}, at $E_{1/2} = -0.43$ to 0.18 V versus NHE (Table 4 and Figures 7 to 9).

Although we are aware of the potential lability of the aqua ligand in **2**, we assume that it is not readily replaced at the ruthenium(III) center under the applied experimental conditions in DMF and DMSO, because (i) the redox potential measured after dissolution of **2** is similar in both DMF and DMSO, and (ii) the electronic absorption spectra of **2** show only minor solvatochromism when DMF, DMSO, or THF were used as a solvent [λ_{max}, nm (ε, mM^{-1} cm^{-1}): 417 (1.4) and 355 (6.1, shoulder) in DMF; 412 (1.7) and 354 (4.3, shoulder) in DMSO; 427 (1.5) and 352 (4.1, shoulder) in THF (see Supporting Information, Table S2)] suggesting the existence of the intact species **2** in these solvents in the timescale of electrochemical measurements. However, RCN readily replaces the aqua ligand at room temperature (see below).

All studied ruthenium(III) complexes undergo solvolysis upon reduction, assignable to cathodically induced metal dechlorination at I^{red} at sufficiently low scan rates, yielding

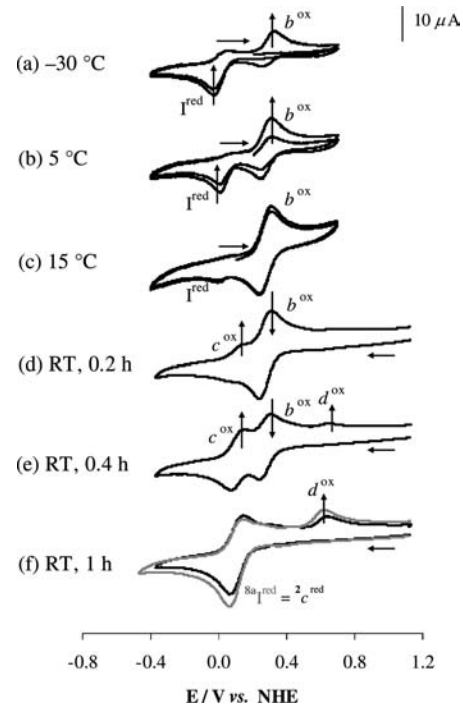

Figure 8. Temperature- and time-dependent solvolytic transformation of **2** (2.0 mM) in 0.20 M [*n*-Bu$_4$N][BF$_4$]/MeCN at a scan rate of 0.20 V s^{-1} at a platinum disk working electrode (see also Scheme 2). The CVs were recorded at (a) −30 °C, (b) 5 °C, and (c) 15 °C, and (d) 0.2 h, (e) 0.4 h, and (f) 1 h after dissolution of **2** in the electrolyte solution at room temperature. Assignment of waves: [Ru^{III}Cl$_3$(Hind)$_2$(H$_2$O)] (**2**, wave I); [Ru^{III}Cl$_3$(Hind)$_2$(MeCN)] (wave *b*); [Ru^{III}Cl$_3$(Hind)(HN=C(Me)ind)] (**8a**, wave *c* for solvolysis product of **2** (^{2}*c* in Figure 8f) or ^{8a}**I** for genuine redox wave of freshly prepared solutions of 8f); [Ru^{II}Cl$_2$(MeCN)(Hind){HN=C(Me)ind}] (wave *d*). In Figure 8f the CV of *mer,trans*-[Ru^{III}Cl$_3$(Hind){HN=C(Me)ind}] (**8a**) is shown in gray.

the mono-DMF or mono-DMSO species detected by the appearance of the oxidation wave *a* at –0.15 to 0.51 in DMF and 0.67 to 0.95 V versus NHE in DMSO (Table 4, Scheme 2). The anodically shifted wave *a* when replacing DMF by DMSO is characteristic for substitution of chlorido ligands by these solvents (see below) and has been studied previously for similar systems.[44,45] The measured redox potentials for **1** and **2** and their reductively induced solvolysis products are in good agreement with those predicted ($E_{1/2}^{pred}$, [Ru^{III}Cl$_4$(Hind)$_2$]$^-$ = −0.39 V; $E_{1/2}^{pred}$, [Ru^{III}Cl$_3$(Hind)$_2$(H$_2$O)] = −0.12 V; $E_{1/2}^{pred}$, [Ru^{II}Cl$_2$(Hind)$_2$(H$_2$O)(DMF)] = 0.15 V; $E_{1/2}^{pred}$, [Ru^{II}Cl$_2$(Hind)$_2$(H$_2$O)(*S*-DMSO)] = 0.67 V vs NHE) by application of Lever's parametrization approach;[46] $E_{1/2}^{pred} = S_M \cdot \Sigma E_L + I_M$ [S_M (0.97), I_M (0.04 V), E_L(Cl$^-$) =

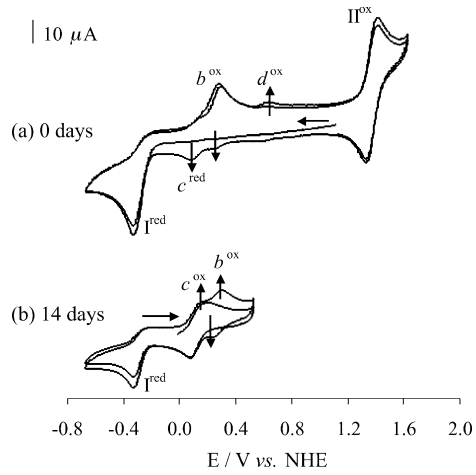

Figure 9. CVs of 2.0 mM Na[*trans*-$RuCl_4(Hind)_2$]·$1.5H_2O$ (**1a**) in 0.20 M [*n*-Bu_4N][BF_4]/MeCN at a scan rate of 0.20 V s^{-1} at a platinum disk electrode recorded (a) immediately and (b) 14 days after dissolution in the electrolyte solution at room temperature. The Ru^{IV}/Ru^{III} redox process for **1a** is shown as wave II and for assignment of the other waves see text, caption of Figure 8, and Scheme 2.

Scheme 2. Proposed Solvolytic Behavior of **2** in DMF and DMSO (top) and MeCN (bottom)

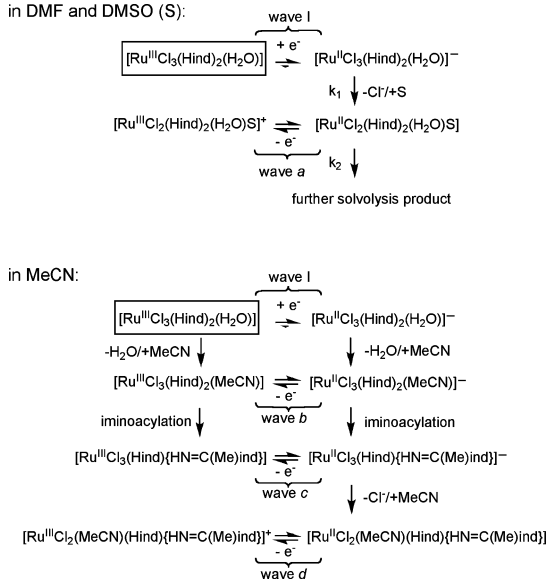

-0.24,[46] $E_L(DMF) = 0.03$,[47] $E_L(H_2O) = 0.04$,[46] $E_L(Hind) = 0.26$,[44] $E_L(S\text{-DMSO}) = 0.57$ V[48]]. Solvolytic replacement upon reduction of the aqua ligand by the solvent DMF would only result in a marginal change in redox potential (similar net donor properties of DMF and H_2O). The observed anodic redox potential shift [$E_{1/2}$ (wave *a*) minus $E_{1/2}$ (I^{red}); Table 4] for **2** is 0.37 V. Therefore, we suggest that a chlorido and not an aqua ligand is replaced by the solvent upon reduction. The higher redox potential of **2** compared to **1** is interesting with respect to our previous finding that an increasing redox potential results in enhanced antineoplastic activity for a series of indazole-based ruthenium complexes.[49] However, extrapolation to aqueous medium is difficult and should be made with caution, in particular, with respect to the complex net charge.[8] Aquation of *trans*-$[Ru^{III}Cl_4(Hind)_2]^-$ (**1**; $E_{1/2}^{exp} = 0.03$ V vs NHE at pH 7.0)[44] gives **2** with pH dependent redox potential (deprotonation of the aqua ligand) in aqueous medium. The 1− net charged hydroxo-species *mer,trans*-$[Ru^{III}Cl_3(OH)(Hind)_2]^-$ [$E_{1/2}^{pred} = -0.24$ V vs NHE, $^{aq,1-/2-}S_M = 0.88$,[44] $^{aq,1-/2-}I_M = 0.46$ V,[44] $E_L(OH^-) = -0.59$ V[46]] would presumably be reduced at a significantly lower redox potential than **1** and **2**.

Upon decreasing the scan rate, an increasing conversion upon reduction at I^{red} of **2** in DMF into $[Ru^{II}Cl_2(Hind)_2(H_2O)(DMF)]$ (Scheme 2) takes place. The first order (no significant variation upon changing the complex concentration) kinetic rate constants for the first (k_1) and second (k_2) steps of solvolysis upon reduction have been investigated by digital simulations. A good fit was obtained for a number of simulations on several CVs (Figure 7). The optimized value of the homogeneous rate constant k_1 for the first ligand-replacement by DMF is 0.24 ± 0.02 s^{-1}, and the second (k_2) is smaller than 0.03 s^{-1}. These values for k_1 and k_2 are significantly lower than those for the nonhydrolyzed complex **1** ($k_1 = 80$ s^{-1}, $k_2 = 0.5$ s^{-1})[44] and higher than those for *mer*-$[Ru^{III}Cl_3(Hind)_3]$ ($k_1 = 0.07$ s^{-1}, $k_2 < 0.03$ s^{-1}).[45] This is in agreement with the reported increase of the homogeneous rate constants of dechlorination upon reduction with a decrease of the redox potential of the corresponding complex.[45]

In MeCN and PhCN the solvolytic behavior of complex **2** is quite different and more complicated (with and without electron-transfer) (Scheme 2). In acetonitrile solutions at −30 °C the electrochemical response of **2** (Figure 8a) is similar to that in DMF and DMSO, although reductively induced solvolysis upon $Ru^{III} \rightarrow Ru^{II}$ reduction yields $[Ru^{II}Cl_3(Hind)_2(MeCN)]^-$ at $E_{1/2} = 0.28$ V versus NHE [$E_{1/2}^{pred}$, $[Ru^{III}Cl_3(Hind)_2(MeCN)] = 0.18$ V (see below); $E_L(MeCN) = 0.34$[46]] detected as wave *b* (in contrast to DMF, where presumably chlorido is replaced by the solvent). The redox potential of $[Ru^{III}Cl_3(Hind)_2(MeCN)]$ (wave *b*) was confirmed by *in situ* generation upon $Ru^{III} \rightarrow Ru^{II}$ reduction of $[RuCl_4(Hind)_2]^-$ in MeCN (Figure 9, see below)]. Whereas the CVs of **2** in DMF suffer only minor alterations when increasing the temperature of the electrolyte solution from −30 °C to room temperature (with the expected increase of the kinetic rate constants k_1 and k_2 in DMF ($^{l}i_p^{ox}/^{l}i_p^{red} = 1.0$ at $T \leq -10$ °C at $v = 0.20$ V s^{-1}), the aqua ligand in **2** is replaced in MeCN (no electron transfer) yielding $[Ru^{III}Cl_3(Hind)_2(MeCN)]$ (wave *b*) at temperatures higher than −5 °C (Figure 8b,c). The UV—vis spectra of **2** recorded

(43) Schumann, H.; Albrecht, I.; Loebel, J.; Hahn, E.; Hossain, M. B.; van der Helm, D. *Organometallics* **1986**, *5*, 1296–1304.
(44) Reisner, E.; Arion, V. B.; Guedes da Silva, M. F. C.; Lichtenecker, R.; Eichinger, A.; Keppler, B. K.; Kukushkin, V.Yu.; Pombeiro, A. J. L. *Inorg. Chem.* **2004**, *43*, 7083–7093.
(45) Reisner, E.; Arion, V. B.; Eichinger, A.; Kandler, N.; Giester, G.; Pombeiro, A. J. L.; Keppler, B. K. *Inorg. Chem.* **2005**, *44*, 6704–6716.
(46) Lever, A. B. P. *Inorg. Chem.* **1990**, *29*, 1271–1285 (accessed May 21, 2008).
(47) A.B.P. Lever; homepage: http://www.chem.yorku.ca/profs/lever/.
(48) Guedes da Silva, M. F. C.; Pombeiro, A. J. L.; Geremia, S.; Zangrando, E.; Calligaris, M.; Zinchenko, A. V.; Kukushkin, V. Yu. *Dalton Trans.* **2000**, 1363–1371.
(49) Jakupec, M. A.; Reisner, E.; Eichinger, A.; Pongratz, M.; Arion, V. B.; Galanski, M.; Hartinger, C. G.; Keppler, B. K. *J. Med. Chem.* **2005**, *48*, 2831–2837.

at room temperature in DMF, DMSO, and THF (see above and Supporting Information, Table S2) differ from those measured in MeCN [λ_{max}, nm (ε, mM^{-1} cm^{-1}): 332 (3.6, shoulder), 375 (6.0), 431 (1.5, shoulder)] indicating a rapid chemical transformation of **2** in acetonitrile. Therefore, dissolution of **2** at room temperature in MeCN is followed by fast solvolysis precluding the accurate detection of the genuine redox couple of **2** by CV and only the acetonitrile species (wave *b*) is present in solution (in contrast to the behavior in DMF or DMSO, where **2** is stable within several hours). After about 10 min at room temperature, a new species (wave *c*, $E_{1/2}$ = 0.12 V vs NHE) emerges (Figure 8d,e), which is the only electroactive species present in solution after 1.5 h (Figure 8f). The cyclic voltammetric response of the new species formed from **2** (at wave ^2c) is identical to that of **8a** in MeCN ($^{8a}I^{red}$; Figure 8f, gray line), which is stable in the electrolyte solution within days. Thus, the species detected at wave *c* is the product of metal-assisted iminoacylation of indazole. The UV−vis spectrum of acetonitrile solution of **2** measured 1 h after dissolution resembles the spectrum of **8a** measured in the same solvent (Supporting Information, Table S3) confirming the formation of the amidine-complex upon solvolysis. In addition, $[Ru^{II}Cl_2(MeCN)(Hind)\{HN{=}C(Me)ind\}]$ is detected (wave *d*) upon $Ru^{III}\rightarrow Ru^{II}$ reduction of **8a**.

In comparison Na[*trans*-$Ru^{III}Cl_4(Hind)_2]\cdot 1.5H_2O$ (**1a**) undergoes replacement of one chlorido ligand by the solvent upon $Ru^{III}\rightarrow Ru^{II}$ reduction in MeCN. The cathodic shift of 0.54 V is in agreement with the reported[50] cathodic shift (0.6 V) for the replacement of one chlorido ligand by a nitrile suggesting the formation of $[Ru^{II}Cl_3(Hind)_2(MeCN)]^-$ (wave *b*, $E_{1/2}$ = 0.28 V vs NHE) and its fast conversion into $[Ru^{II}Cl_3(Hind)\{HN{=}C(Me)ind\}]^-$ (wave *c*, $E_{1/2}$ = 0.12 V vs NHE, Figure 9a). The solvolytic behavior (no electron transfer) of Na[*trans*-$Ru^{III}Cl_4(Hind)_2]\cdot 1.5H_2O$ (**1a**) is similar to that of **2**, but the chlorido ligands are considerably more inert than the aqua ligand in **2** resulting in a slower solvolysis of the former complex. Running a CV 3−4 days after dissolution shows the formation to some extent of the amidine species **8a** (wave *c*). After 2 weeks about half the amount of **1a** has converted into **8a** ($^{I}i^{red}/^{c}i^{ox}$ close to unity, Figure 9b). The rate determining step in the formation of the amidine is the iminoacylation of indazole for **2**, whereas it is the solvolysis to the mononitrile species for the tetrachlorido complex **1**. The more positive $E_{1/2}$ value of **8b** than **8a** (Table 4) is in agreement with the more electron-withdrawing properties of the phenyl moiety in **8b** resulting in a higher effective charge on the Ru^{III} center in **8b** compared to **8a** (electron donating methyl group).

Final Remarks. Aquation of the anticancer drug *trans*-$[Ru^{III}Cl_4(Hind)_2]^-$ (**1**, KP1019) resulted in the formation of the reactive species *mer,trans*-$[Ru^{III}Cl_3(Hind)_2(H_2O)]$ (**2**) with a labile Ru—OH_2 bond. In the present work the solvolytic reactions of **1** and **2**, which previously were not understood in detail, have been investigated. Solvolysis in different solvents showed a variety of reaction pathways, which are initiated by easy release of the aqua ligand: (i) in weakly coordinating solvents (e.g., acetone) dimerization of **2** occurs to give $[Ru_2^{III}(\mu\text{-}Cl)_2Cl_4(Hind)_4]$ (**3**) with release of H_2O, (ii) in the presence of stronger donor molecules the aqua ligand is replaced by the solvent to give complexes *mer,trans*-$[Ru^{III}Cl_3(Hind)_2(S)]$ (**4**, S = MeOH) and **5** (S = Me_2S)), (iii) in nitrile solvents fast insertion of the solvent in the N—H bond of indazole in **2** resulted in ruthenium(III)-assisted iminoacylation of the azole to give complexes *mer*-$[Ru^{III}Cl_3(Hind)\{HN{=}C(R)ind\}]$ [**8a** (R = Me), **8b** (R = Ph)] and $[Ru^{III}Cl_2\{HN{=}C(Me)ind\}_2]Cl$ (**9**). Electrochemical studies showed the formation of transient species $[Ru^{III}Cl_3(Hind)_2(MeCN)]$ and $[Ru^{III}Cl_2(Hind)\{HN{=}C(Me)ind\}(MeCN)]$ with activated MeCN via coordination prior to the iminoacylation, which then led to the amidine metallocycle. Ruthenium(III)-promoted iminoacylation of azoles is unprecedented as well as two consecutive iminoacylations of indazoles at one metal center. Taking into account the very low solubility of **2** in water and its high reactivity, one can suppose that in vivo this aquo intermediate does not accumulate but readily reacts.

Aquation of **1** results in a significant anodic shift of $E_{1/2}$ in organic solvents. A higher redox potential should result in easier reduction in vivo and formation of reactive ruthenium(II) species to attack biological targets. The DNA model bases 9-meade and 6-me_2ade coordinate to the ruthenium center via N7 (**10**) and N3 (**11**), respectively, the latter being a potential alternative binding site to the commonly observed metalation of the N7 position. Although the more labile character of the Ru—OH_2 bond in **2** than the Ru—Cl bond in **1** has been qualitatively established in this work, studies are under way in our laboratory to investigate quantitatively differences in reactivity of **1** and **2** toward biologically relevant molecules.

Acknowledgment. The authors are indebted to the FWF (Austrian Science Fund), to the Austrian Council for Research and Technology Development, to the Austrian Research Promotion Agency (FFG) and COST (European Cooperation in the Field of Scientific and Technical Research) for financial support. We also thank A. Egger for helpful hints for the synthesis of **11** and Prof. G. Giester for X-ray data collection of compound **11**·THF.

Supporting Information Available: Hydrogen bonds and their geometrical parameters in the crystal structure of complex **2**, **8a**·Et_2O, and **8b**·PhCN, UV−vis data of complexes **1**−**4**, **8a**, **8b**, **9**, and **11** in different solvents, scheme of the proposed mechanism for the reaction of iminoacylation in **1** and **2** (PDF), and the crystallographic tables and X-ray crystallographic files in CIF format for complexes **2**, **4**·MeOH, **8a**·Et_2O, **8b**·PhCN, **9**·MeCN, **11**·THF, and **12**. This material is available free of charge via the Internet at http://pubs.acs.org.

IC800506G

(50) Duff, C. M.; Heath, G. A. *J. Chem. Soc., Dalton Trans.* **1991**, 2401–2411.